

# A new anode material for oxygen evolution in molten oxide electrolysis

Antoine Allanore<sup>1</sup>, Lan Yin<sup>1†</sup> & Donald R. Sadoway<sup>1</sup>

Molten oxide electrolysis (MOE) is an electrometallurgical technique that enables the direct production of metal in the liquid state from oxide feedstock<sup>1,2</sup>, and compared with traditional methods of extractive metallurgy offers both a substantial simplification of the process and a significant reduction in energy consumption<sup>3</sup>. MOE is also considered a promising route for mitigation of CO<sub>2</sub> emissions in steelmaking<sup>3–5</sup>, production of metals free of carbon<sup>6</sup>, and generation of oxygen for extra-terrestrial exploration<sup>7,8</sup>. Until now, MOE has been demonstrated using anode materials that are consumable (graphite for use with ferro-alloys and titanium<sup>6,9</sup>) or unaffordable for terrestrial applications (iridium for use with iron<sup>10,11</sup>). To enable metal production without process carbon, MOE requires an anode material that resists depletion while sustaining oxygen evolution. The challenges for iron production are threefold. First, the process temperature is in excess of 1,538 degrees Celsius (ref. 10). Second, under anodic polarization most metals inevitably corrode in such conditions<sup>11–13</sup>. Third, iron oxide undergoes spontaneous reduction on contact with most refractory metals<sup>14</sup> and even carbon. Here we show that anodes comprising chromium-based alloys exhibit limited consumption during iron extraction and oxygen evolution by MOE. The anode stability is due to the formation of an electronically conductive solid solution of chromium(III) and aluminium oxides in the corundum structure. These findings make practicable larger-scale evaluation of MOE for the production of steel, and potentially provide a key material component enabling mitigation of greenhouse-gas emissions while producing metal of superior metallurgical quality.

Alloys of composition Cr<sub>1–x</sub>Fe<sub>x</sub> have been tested as bulk anode materials under electrochemical conditions previously demonstrated

as successful for iron extraction<sup>10</sup>. The mass fraction of iron in the alloy has been varied between 0 and 30% (that is, *x* between 0 and 0.3), the iron-rich limit corresponding to an alloy melting point equal to the process temperature (1,600 °C). The selected electrolyte composition is very basic, which is advantageous for its physico-chemical properties—for example, electrical conductivity and viscosity—but challenging in terms of anode materials compatibility<sup>11</sup>.

The electrolysis cell, operated in constant-current mode (Fig. 1a) at an average anode current density exceeding 2 A cm<sup>–2</sup>, exhibited a low cell voltage, which reached a steady value of around 3.8 V after slightly less than 2 h. Increasing the current density does not lead to an intolerable increase in the cell voltage, although there is an increase in its amplitude of variation. Observation of the electrolyte surface close to the anode during electrolysis confirms the evolution of gas (Supplementary Video), the generation and accumulation of which in such a small cell have a noticeable impact on the variation of voltage with time. The fact that the oxygen content of the outlet gas gradually reaches values comparable to those observed with a noble-metal anode in the same cell<sup>11</sup> is evidence of successful production of oxygen with this new anode material. Its measured faradaic efficiency—based on the recovered oxygen and taking into account typical consumption by oxidation of the inactive parts of the furnace (mainly the molybdenum current collectors)—is around 24%, similar to that previously obtained with an iridium anode. Furthermore, the oxygen concentration in the process off-gas scales with current density. The simultaneous production of metal is confirmed by the observation of the cathode after electrolysis (Fig. 1b). The iron metal, which has alloyed with the molybdenum cathode substrate, contains almost no carbon (<25 p.p.m.), a small amount of chromium (<500 p.p.m.), and an amount of

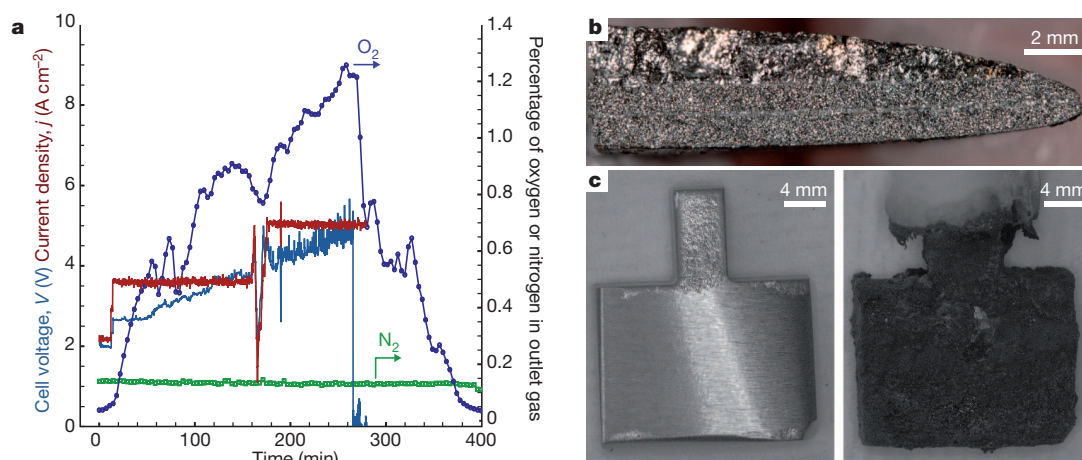


**Figure 1 | Electrolysis experiments demonstrate metal and oxygen production with a macroscopically stable Cr<sub>90</sub>Fe<sub>10</sub> anode.** a, Variation of the cell voltage (left axis) and oxygen and nitrogen content of the process gas (right) during constant-current electrolysis ( $T = 1,565$  °C, 92,964 C). b, Fracture of the

cathode deposit, showing the deposition of molten metal on top of the substrate. c, Macrographs of a Cr<sub>90</sub>Fe<sub>10</sub> anode before (left) and after (right) electrolysis, showing the limited change in dimensions ( $T = 1,565$  °C, 21,923 C).

<sup>1</sup>Department of Materials Science and Engineering, Massachusetts Institute of Technology, Cambridge, Massachusetts 02139-4307, USA. †Present address: Department of Materials Science and Engineering, University of Illinois Urbana-Champaign, Urbana, Illinois 61801, USA.

oxygen in agreement with that predicted by thermodynamics for carbon-free iron at 1,600 °C (<4,000 p.p.m.). At the cathode the corresponding faradaic efficiency is 34%, in close agreement with previous investigations<sup>10,11</sup>. Along with these promising electrochemical results, anode stability has been demonstrated (Fig. 1c): the external dimensions have barely been affected by electrolysis, as confirmed by repeated testing for various durations with a plurality of alloy compositions (Supplementary Fig. 1). The anode shows coverage by electrolyte (so-called drag-out) that has adhered to the surface.

The efficiency and stability of the  $\text{Cr}_{1-x}\text{Fe}_x$  alloys for oxygen evolution is in agreement with thermodynamic calculations, which predict the solid chromium(III) oxide product to be stable in molten electrolyte (Supplementary Discussion A, Supplementary Fig. SA2). However, a study of the anode microstructure after electrolysis (Fig. 2a and Supplementary Fig. 2) suggests a more sophisticated mechanism. First, limited internal oxidation of the alloy is observed together with chromium depletion in the bulk metal of ~10%, effective over a distance of approximately 150  $\mu\text{m}$  (Fig. 2b). Second, and of relevance to the overall anode stability, a triplex scale is observed at the alloy surface: metal oxide/mixed oxide/frozen electrolyte. Analysis by energy dispersive spectroscopy (EDS; Fig. 2a) and optical observations under polarized light (Fig. 2c) reveal that the oxidation products are found in two layers: an inner layer of chromium oxide ( $\text{Cr}_2\text{O}_3$ ) containing a few per cent of aluminium, and an outer layer composed of a solid solution of  $\text{Cr}_2\text{O}_3$  and  $\text{Al}_2\text{O}_3$ .

The crystallographic structures of these phases have been confirmed by X-ray diffraction (XRD) analysis of the inner side of the crust (Fig. 2d, measured from the alloy side) and the powder obtained by crushing the entire crust (Fig. 2e). In the latter, a signal from the frozen

slag is also noticeable. A small amount of chromium has been found in the electrolyte close to the anode (Fig. 2a), in agreement with both the thermodynamic prediction and the experimental measurements of chromium oxide chemical solubility in an oxide melt of this specific composition (Supplementary Discussion A). The composition and morphology of the oxide scale were found to be pretty much independent of the composition of the base alloy, which influenced mainly the extent of chromium depletion (Supplementary Fig. 2). In the case of pure chromium, the inner layer was found to contain a higher concentration of aluminium, and the outer layer exhibited a non-negligible concentration of calcium.

The influence of electrolysis duration on the thickness of the chromium(III) oxide containing layer did not prove to be important (for  $\text{Cr}_{90}\text{Fe}_{10}$ :  $75 \pm 16 \mu\text{m}$  after 2.5 h as compared to  $42 \pm 38 \mu\text{m}$  after 5.2 h) on the timescale investigated, which was limited by the crucible material performance. In contrast, the initial concentration of iron in the anode was found to be of major importance: an anode containing 30% iron in the starting material proved to develop thicker chromium oxide containing layers (for  $\text{Cr}_{70}\text{Fe}_{30}$ :  $115 \pm 26 \mu\text{m}$ ) and to incur higher internal depletion of chromium, leading to the formation of a low melting point alloy responsible for faster local consumption and reshaping of the anode by alloy fusion (Supplementary Figs 1 and 2).

Dry oxidation studies conducted on the same alloys in similar conditions proved that the rate of chromium oxide formation during electrolysis was comparable ( $36 \pm 16 \mu\text{m}$  after 2.5h) and not sensitive to either the oxygen concentration or the alloy iron content (Supplementary Discussion B, Supplementary Figs SB2 and SB3), suggesting that electrolysis did not lead to an inescapable increase in the oxidation rate of the metal. The application of existing oxidation theory (Supplementary

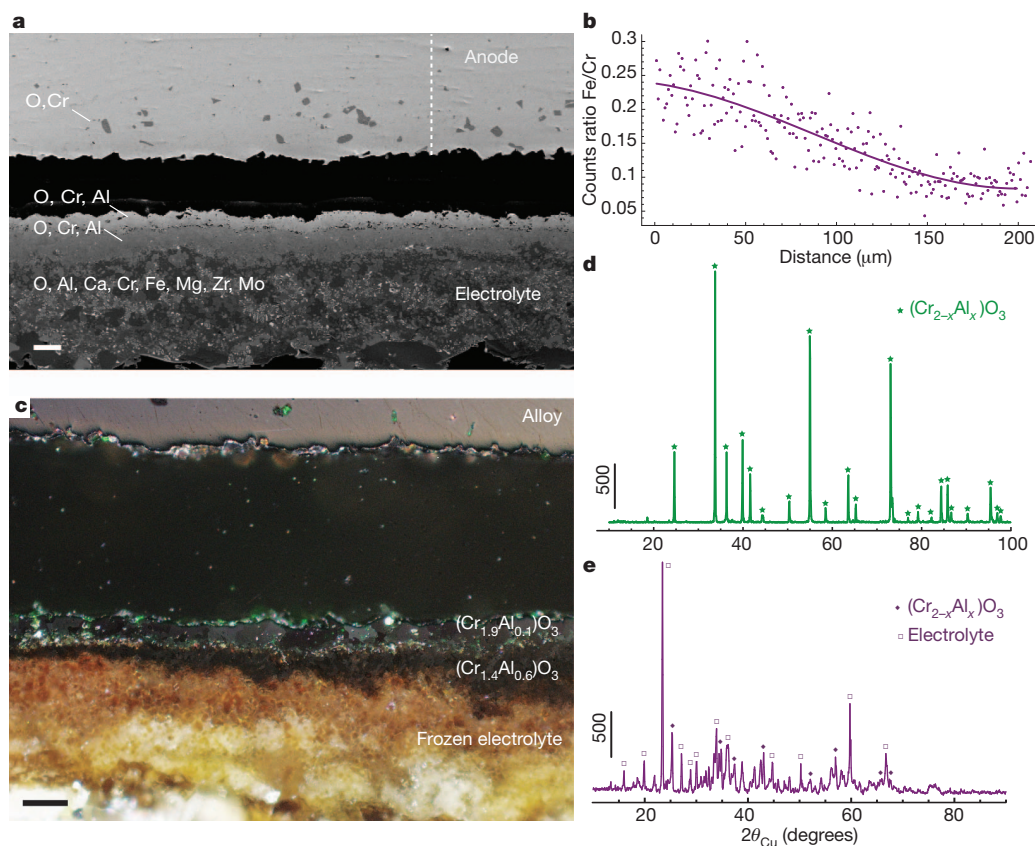


**Figure 2 | Anodes developed passivation layers rich in chromium(III) oxide during electrolysis.** **a**, SEM micrograph in backscattered mode of  $\text{Cr}_{90}\text{Fe}_{10}$  ( $T = 1,565 \text{ }^\circ\text{C}$ , 21,920 C). Elements at left ranked by atomic concentration measured by EDS. The vertical dotted line at right corresponds to the line analysed in **b**. Scale bar, 50  $\mu\text{m}$ . **b**, EDS analysis of Cr/Fe atomic ratio along the

line presented in **a**, revealing chromium depletion towards the surface. **c**, Optical micrograph of the anode/electrolyte interface with phases identified by EDS and XRD. Scale bar, 50  $\mu\text{m}$ . **d**, **e**, XRD spectra of the inner side of the interface (from the alloy side; **d**) and the oxide layers in powdered form (**e**).

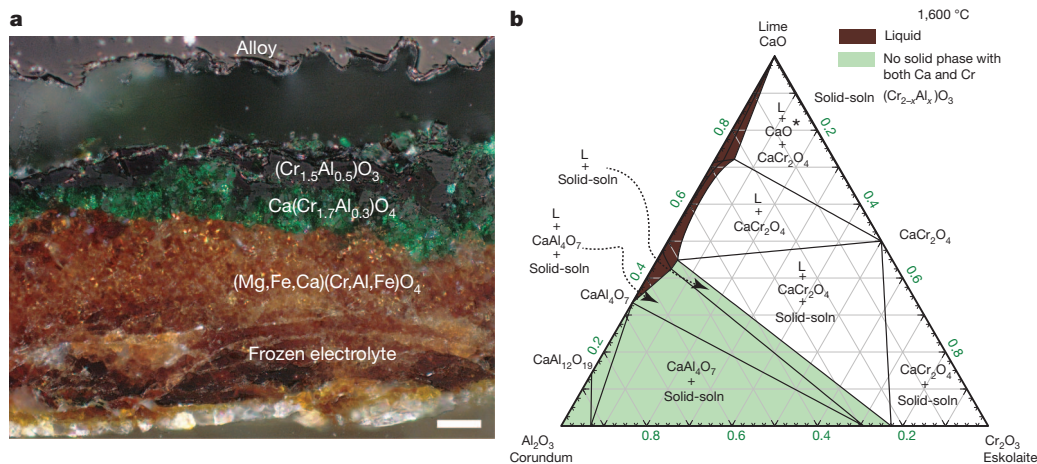


**Figure 3** |  $\text{Cr}_{1-x}\text{Fe}_x$  alloys immersed in electrolyte in the absence of electrolysis develop a mixed oxide layer composed of both calcium spinel and chromia-alumina solid solution. **a**, Optical micrograph of a  $\text{Cr}_{90}\text{Fe}_{10}$  anode after immersion for 5 h in the electrolyte without polarization. Phase identification is based on EDS and XRD analysis. Scale bar, 50  $\mu\text{m}$ . **b**, Phase

Discussion B, Supplementary Fig. SB5) suggests that in this specific electrolysis case, external polarization creates an electric field of such small magnitude across the anode scale as to have almost no influence on the oxide growth rate.

Chromium alloys immersed in the molten electrolyte in the absence of electrolysis (Fig. 3a) proved to develop a thicker layer ( $98 \pm 29 \mu\text{m}$  of chromium-rich oxide layer after 5 h) than in either the electrolysis or the dry oxidation cases. Analysis of the chromium-rich oxide layers also reveals the presence of a calcium spinel phase containing chromium and aluminium (Fig. 3a and Supplementary Discussion A, Supplementary Fig. SA4).

The results obtained after electrolysis show that the oxide scale formed on the alloy is principally a solid solution of chromium(III) oxide and aluminium oxide (alumina), whereas without polarization a calcium spinel phase predominates. The phase diagram for alumina–chromium(III) oxide–calcium oxide (Fig. 3b) confirms that at low calcium oxide concentration, in green on the diagram, the stable chromium-containing solid-oxide phase is indeed the solid solution with alumina. It is likely that electro-migration under the influence of electrolysis is responsible for driving away the positive calcium ions (calcium ion is the dominant cation in the electrolyte, while aluminium is present as an aluminate anion), leading to the formation of a calcium-free solid solution of chromium and aluminium on the anode. From an oxidation perspective, the formation of the solid solution in place of the calcium spinel is seen as beneficial, because chromium diffusivity is expected to be smaller in the corundum structure than in the spinel. The diffusivity of  $\text{Cr}^{3+}$  in the chromium oxide–alumina solid solution is also predicted to be smaller than in a pure chromium oxide phase owing to the difference in lattice constant<sup>15</sup>. Finally, the formation of such a solid solution may also modify the rate-determining step for oxidation, because it has been shown that the oxygen coverage on such material is much poorer than on pure chromium(III) oxide<sup>16</sup>.

These results have two consequences. First, the successful extraction of metal and oxygen obtained with an affordable alloy-based anode material at bench-scale will enable the design of a reactor of sufficiently large scale that longer-term MOE performance can be properly assessed—for example, the specific energy consumption and cell service lifetime. This is especially important in light of the fact that the values of such performance characteristics obtained in the present laboratory-scale cell configuration are not considered to be representative of industrial conditions. The same disparity holds for other high-temperature electrolytic technologies, notably the Hall–Héroult process for extraction of aluminium<sup>17</sup>. Encouraging signs are to be found in the

diagram of chromium(III) oxide, aluminium oxide and calcium oxide at 1,600 °C, predicted from available data. Areas in brown and green represent respectively the liquid phase and the domain of immiscibility of chromium and calcium in a solid oxide phase.  $\text{CrO}_2(\text{s})$  has been removed from the diagram because of its low concentration.  $\text{CaO}^*$  is in the liquid phase.

results of previous large-scale production of manganese by MOE<sup>6</sup>. Second, the oxidation behaviour of alloys in such an extreme environment has resulted in a novel microstructure that challenges high-temperature oxidation theory, that is, the formation of an oxide solid solution containing one element not present in the base alloy. Further work will involve the application of existing passivation theory, for example, the point defect model<sup>18</sup>, to the specific case of molten oxide electrolytes.

## METHODS SUMMARY

The original set-up described elsewhere<sup>11</sup> has been adapted for the investigation of a non-noble metal anode (Methods). In summary, a vertical tube furnace constantly purged with helium is used to maintain the cell temperature. The process outlet gas composition is monitored with a gas chromatograph, which measured an average  $\text{O}_2$  content before electrolysis of around 50 p.p.m. The cell consists in an yttria-stabilized zirconia crucible containing the oxide mixture (in wt%: 42.3 CaO, 42.3  $\text{Al}_2\text{O}_3$ , 5.4 MgO and 10  $\text{Fe}_3\text{O}_4$ ), pre-melted before the electrolysis experiment. All electrodes are immersed into the electrolyte from the top of the furnace, through a gas-tight cap equipped with vacuum-type feedthroughs. The horizontal cathode consists of two molybdenum disks, 3.8 cm in diameter and 0.1 cm thick, attached by nuts of the same material to a threaded molybdenum lead, 0.5 cm in diameter.

The  $\text{Cr}_{1-x}\text{Fe}_x$  alloys were prepared by arc-melting high-purity metals (minimum 99.95% of known weight). Anodes were cut to the required dimensions (typically  $2 \times 1 \times 0.7 \text{ cm}$ ) by water-jet. The anode surfaces were ground by belt sander with no. 220 grit SiC paper before welding. Samples were connected to molybdenum leads, 0.3 cm in diameter and 90 cm long, by tungsten inert gas welding in a box flushed with argon. Evaluation of the dry oxidation features of the alloys under investigation was conducted using a thermogravimetric analyser and vertical tube furnace. Details of observation and characterization methods are provided in Methods.

**Full Methods** and any associated references are available in the online version of the paper.

Received 26 October 2012; accepted 18 March 2013.

Published online 8 May 2013.

- Aiken, R. H. Process of making iron from the ore. US patent 816, 142 (1906).
- Esin, O. A. Electrochemistry of molten oxides. *Zh. Fiz. Khim.* **30**, 3–19 (1956).
- Birat, J.-P., Lorrain, J.-P. & de Lassat, Y. The “CO<sub>2</sub> tool”: CO<sub>2</sub> emissions and energy consumption of existing and breakthrough steelmaking routes. *Rev. Métal.* **106**, 325–336 (2009).
- International Energy Agency. *Energy Technology Perspective* 179–180 (OECD/IEA, Paris, 2010); available at <http://www.iea.org/publications/freepublications/publication/etp2010.pdf>.
- Halper, M. Stainless steel. *Time* **177**, 7–9 (2011).

- Winand, R., Fontana, A., Segers, L., Hannaert, P. & Lacave, J. in *Int. Symp. Molten Salt Electrolysis in Metal Production* 42–50 (Institute of Mining and Metallurgy, London, 1977).
- Oppenheim, M. J. Electrolysis of molten basalt. *Mineral. Mag.* **36**, 1104–1122 (1968).
- Sanderson, F. How to breathe on the moon. *Nature* <http://dx.doi.org/10.1038/news.2009.803> (published online 10 August 2009).
- Sadoway, D. R. Electrochemical processing of refractory metals. *J. Met.* **43**, 15–19 (1991).
- Wang, D., Gmitter, A. J. & Sadoway, D. R. Production of oxygen gas and liquid metal by electrochemical decomposition of molten iron oxide. *J. Electrochem. Soc.* **158**, E51–E54 (2011).
- Kim, H., Paramore, J., Allanore, A. & Sadoway, D. R. Electrolysis of molten iron oxide with an iridium anode: the role of electrolyte basicity. *J. Electrochem. Soc.* **158**, E101–E105 (2011).
- Sadoway, D. R. Inert anodes for the Hall-Héroult cell: the ultimate materials challenge. *J. Met.* **53**, 34–35 (2001).
- Di Martino, J., Rapin, C., Berthod, P., Podor, R. & Steinmetz, P. Corrosion of metals and alloys in molten glasses. Part 2: nickel and cobalt high chromium superalloys behaviour and protection. *Corros. Sci.* **46**, 1865–1881 (2004).
- Carton, A., Rapin, C., Podor, R. & Berthod, P. Corrosion of chromium in glass melts. *J. Electrochem. Soc.* **153**, B121–B127 (2006).
- Takahashi, N. T., *et al.* Cr diffusion in  $\alpha$ -Al<sub>2</sub>O<sub>3</sub>: secondary ion mass spectroscopy and first-principles study. *Phys. Rev. B* **82**, 174302 (2010).
- Egerton, T. A., Stone, F. S. & Vickerman, J. C.  $\alpha$ -Cr<sub>2</sub>O<sub>3</sub>-Al<sub>2</sub>O<sub>3</sub> solid solutions 1. The formation and stability of adsorbed oxygen. *J. Catal.* **33**, 299–306 (1974).
- Nguyen, T. & de Nora, V. in *Light Metals* (ed. Galloway, T. J.) 385–390 (The Minerals, Metals and Materials Society, 2006).
- MacDonald, D. The history of the point defect model for the passive state: a brief review of film growth aspects. *Electrochim. Acta* **56**, 1761–1772 (2011).

**Supplementary Information** is available in the online version of the paper.

**Acknowledgements** The financial support of the American Iron and Steel Institute is acknowledged; we thank H. Kim and J. Paramore for assistance with the experimental set-up and for discussions.

**Author Contributions** A.A. conceived the idea and designed the study based on principles enunciated by D.R.S. A.A. and Y.L. performed the experiments, the analysis of the results, and wrote the original draft of the paper. D.R.S. edited the original manuscript and revised it for submission. All authors discussed the results and commented on the paper.

**Author Information** Reprints and permissions information is available at [www.nature.com/reprints](http://www.nature.com/reprints). The authors declare no competing financial interests. Readers are welcome to comment on the online version of the paper. Correspondence and requests for materials should be addressed to A.A. ([allanore@mit.edu](mailto:allanore@mit.edu)).

## METHODS

**Electrolysis experiments.** The electrolyte chosen for electrolysis was composed of multiple oxides (CaO, MgO, Al<sub>2</sub>O<sub>3</sub>), in which 10 wt% of magnetite (Fe<sub>3</sub>O<sub>4</sub>) was added as iron oxide feedstock. The composition and properties of the electrolyte have been provided elsewhere<sup>11</sup>. The high concentration of ionic compounds—mainly calcium oxide—is responsible for some important features of this electrolyte for electrolysis: for example, high electrical conductivity; low melting point, and low density and viscosity. The oxide powders were purchased from laboratory chemicals suppliers, with purity higher than 99 wt%. These powders were mixed in a polyethylene bottle and pre-melted in sacrificial magnesia crucibles to reduce experimental artefacts. This step has been identified as crucial for successful anode stability: if not removed before the electrolysis, impurities entrapped in the oxide compounds, such as water, were released during furnace ramping and led to contamination of the anode surface, leading to poor performance during electrolysis.

Ytria-stabilized zirconia crucibles (5 wt% Y<sub>2</sub>O<sub>3</sub>, 6.6 cm diameter, 10.5 cm height, Jiangsu Province Ceramic) were used as the electrolyte container. A high-purity magnesia crucible (99.8 wt%, Ozark Technical Ceramics) was used as a secondary container to protect the tube furnace in case of failure of the inner zirconia crucible.

Chromium alloyed with 0 to 30 wt% iron (Cr<sub>1-x</sub>Fe<sub>x</sub> alloy, *x* ranging from 0 to 0.30), has been assessed for its suitability as an oxygen-evolving anode. Strips of 1 cm thickness of these alloys were provided by Ames National Laboratory (Ames, Iowa, USA); they were obtained by arc melting in an argon atmosphere and were cut into coupons by water jet to typically 2.0 × 1.0 × 0.7 cm with a top-pin of around 1.0 × 0.5 × 0.7 cm for welding. The surface of the anode was polished with no. 220 SiC papers. The pin of the anode was welded to a molybdenum rod (0.3 cm diameter, 90 cm height, American Elements) that served as a current lead. Two molybdenum disks of 0.1 cm thickness and 3.8 cm diameter served as the cathode. These disks were connected to a threaded molybdenum rod by molybdenum nuts. Molybdenum leads were protected by high-purity alumina tubes, and high-purity alumina paste (Resbond 989, Cotronics Corp.) was used to protect connections in the head space above the electrolyte. The immersed part of the cathode lead was protected with an extra magnesia or zirconia tube. The anode was held vertically above the horizontal cathode disk, the corresponding projected anode area on the cathode being typically 1.4 cm<sup>2</sup>. This value was used in the estimation of anodic current densities.

The high-temperature pre-oxidation of the anode alloys as well as the electrolysis experiments were conducted in a vertical tube furnace fitted with lanthanum chromite heating elements (model PVT 18/100/350 with 3216P1 controller, Carbolite) and a closed-one-end alumina tube (11.4 cm inner diameter, 1 m height, 99.8%, McDanel Advanced Ceramics).

The crucible containing solid pre-melted electrolyte was placed in the hot zone of the furnace tube, the two electrodes being suspended above the crucible contents during ramping of the temperature.

High-purity helium was continuously flowed through the tube furnace at a rate of 250 cm<sup>3</sup> STP min<sup>-1</sup> to maintain an inert atmosphere. The oxygen content of the process outlet gas was analysed by gas chromatography (CP-4900 Micro-Gas Chromatograph, Varian Inc.) and was measured to contain less than 50 p.p.m. oxygen during furnace temperature ramping and before electrolysis. The continuous monitoring of the oxygen level and the gas flow-rate at the reactor outlet allow

us to estimate the anodic faradaic efficiency specific to this laboratory configuration. It is necessary, however, to be aware of the limitation of this method, because part the oxygen is consumed by the oxidation of the metallic parts present into the tube furnace, in particular by the molybdenum current collectors. A control experiment was conducted in which a known quantity of oxygen was injected at the inlet (1% O<sub>2</sub> in He at 300 cm<sup>3</sup> STP min<sup>-1</sup>). The corresponding oxygen level at the reactor outlet (0.5%) suggested that around one-half of the oxygen could be consumed by internal oxidation. This 50% loss in measuring the oxygen outlet concentration has been taken into account in the anodic faradaic efficiency estimates reported in the main text. The cathode efficiency has been estimated by chemical titration (ICP-OES) of the iron content of one-quarter of the molybdenum disc cathode after electrolysis. The first set point of the furnace was 1,450 °C with a ramping rate of 1.5 °C min<sup>-1</sup>, followed by dwelling for 2 h. This first step allowed pre-oxidation of the anode and the formation of a protective chromium(III) oxide layer on the anode surface. The second set point was 1,600 °C, the temperature at which the cathode was immersed 3 cm into the electrolyte. The anode was lowered afterwards under anodic polarization (constant cell voltage of 2 V) by 1 cm. A type-B thermocouple was also positioned above the molten electrolyte level to monitor the process temperature: 1,565 °C for a furnace set point of 1,600 °C. Galvanostatic electrolysis (Argantix XDS30-500-208IF, California Instruments Corp.) was conducted at currents ranging from 2 A to 9 A for a duration ranging between 1.5 and 6 h. After electrolysis, both electrodes were raised out of the melt to a relatively cold zone in the furnace to preserve the reaction products.

**Dry oxidation experiments.** Oxidation experiments were carried out both in a thermogravimetric (TG) analyser (Netzsch STA 409) and the vertical tube furnace. The TG samples were Cr<sub>1-x</sub>Fe<sub>x</sub> alloy beads of around 200 mg produced by arc-melting in argon atmosphere. Oxidation of Cr<sub>1-x</sub>Fe<sub>x</sub> (*x* = 0.1, 0.2 and 0.3) alloys at 1,600 °C in Ar for 3 h was investigated in the tube furnace, emulating the electrolysis process. Each sample was submitted to the same preparation and experimental procedure as that for electrolysis.

**Chromium(III) oxide stability experiments.** The Cr<sub>90</sub>Fe<sub>10</sub> alloy (same as that for electrolysis) and sintered Cr<sub>2</sub>O<sub>3</sub> pellets were used to study the stability of Cr<sub>2</sub>O<sub>3</sub> in molten electrolyte at 1,600 °C in the absence of polarization using the vertical tube furnace.

**Post-experiment observations and analysis.** The samples were disassembled for detailed characterization at room temperature. Part of the crust on the alloy surface was peeled off for SEM-EDS analysis (Leo VP438) on both inner and outer surfaces. Various phases on the inner surface, outer surface, and in the bulk of the crust after crushing to powder were identified by X-ray diffraction (X'Pert Pro Multipurpose Diffractometer, PANalytical). Cross-sections were obtained by mounting in thermosetting polymer, cutting with a diamond saw, and polishing with SiC papers and diamond solution down to 1 μm. A high-magnification optical microscope (Olympus GX51) and SEM were used to investigate the cross-sectional surface. The carbon content of the iron product on the cathode was measured by the Leco combustion technique. Direct current plasma coupled with atomic emission spectroscopy was used to analyse the iron, chromium and molybdenum contents of the cathode deposit.

**Statistics.** Oxide layer thicknesses in the text are given as (mean ± standard deviation) based on measurements at 10 locations along the layer.